Polymer 50 (2009) 560–568

Contents lists available at ScienceDirect

Polymer

journal homepage: www.elsevier.com/locate/polymer

Hollow polymeric microcapsules: Preparation, characterization and application in holding boron trifluoride diethyl etherate

Ding Shu Xiao [a], Yan Chao Yuan [a], Min Zhi Rong [b,*], Ming Qiu Zhang [b]

[a] Key Laboratory for Polymeric Composite and Functional Materials of Ministry of Education, OFCM Institute, School of Chemistry and Chemical Engineering, Zhongshan University, Guangzhou 510275, PR China
[b] Materials Science Institute, Zhongshan University, Guangzhou 510275, PR China

ARTICLE INFO

Article history:
Received 11 April 2008
Received in revised form
11 November 2008
Accepted 13 November 2008
Available online 25 November 2008

Keywords:
Hollow microcapsules
Boron trifluoride diethyl etherate
Infiltration

ABSTRACT

A novel method was proposed to prepare boron trifluoride diethyl etherate ($(C_2H_5)_2O\cdot BF_3$)-loaded microcapsules. To protect the high activity of $(C_2H_5)_2O\cdot BF_3$, hollow microcapsules were prepared via UV-initiated polymerization in emulsion with the aid of CO_2 microbubble templates, evacuation, and immersion in $(C_2H_5)_2O\cdot BF_3$ allowing infiltration of the chemical. The selected photo-initiator induced rapid curing of the oil layer in the CO_2/oil/water emulsion, ensuring production of the desired hollow capsules. Structure, geometry, morphology and properties of the resultants were carefully studied in relation to their synthesis conditions and loading behavior in liquid $(C_2H_5)_2O\cdot BF_3$. The results indicated that the amount of $(C_2H_5)_2O\cdot BF_3$ filled in the capsules can be adjusted by changing the shell composition. Having been encapsulated, $(C_2H_5)_2O\cdot BF_3$ maintained its reactivity with epoxy.

1. Introduction

Self-healing of cracks in polymers and polymer composites has attracted more and more research interests of materials scientists [1,2]. Recently, the strategy based on microencapsulation, proposed by White and co-workers [3–16], opened a new road towards practical application of the technique. The principle lies in the fact that healing agent is encapsulated and embedded in the materials in advance. As soon as cracks destroy the fragile capsules, the healing agent would be released into the crack planes due to capillary effect and then polymerized, so that the cracks can be re-bound. Taking the advantage of microencapsulation, healing agent is well protected from composites manufacturing and comes into effect only upon cracking.

In our laboratory, self-healing epoxy composites were prepared, in which microencapsulated epoxy served as the polymerizable component of the healant [17–19]. Due to the nature of the mate hardener (i.e. imidazole), self-repairing operation against cracks has to be conducted at elevated temperature. To provide the composites with healing ability without the requirement of manual intervention, highly active hardeners, such as amine, thiols and boron trifluoride diethyl etherate ($(C_2H_5)_2O\cdot BF_3$), should be used. Unlike the epoxy-loaded microcapsules that have been intensively studied [20–23], however, microencapsulation of these active chemicals is very difficult, because they would be easily deactivated during encapsulation processes.

In terms of modified in-situ polymerization of melamine-formaldehyde in an oil-in-water emulsion, we have successfully synthesized poly(melamine-formaldehyde) (PMF)-walled microcapsules containing polythiol [24]. The capsules proved to be qualified for acting as the mate of epoxy in making two-part microencapsulated healing agent of self-healing epoxy composites [25]. Because epoxy–thiol cure is a nucleophilic addition reaction, both the epoxy- and thiol-loaded capsules should be homogeneously mixed at the stoichiometric ratio for obtaining high healing efficiency. In this context, replacement of thiol with $(C_2H_5)_2O\cdot BF_3$ as core substance in the hardener capsules might be more attractive. $(C_2H_5)_2O\cdot BF_3$ used to be a curing agent for low temperature fast cure epoxy adhesives. As the reaction between epoxy and $(C_2H_5)_2O\cdot BF_3$ belongs to cationic polymerization, curing of the liberated epoxy from the broken microcapsules would spread out quickly so long as the epoxy fluid meets $(C_2H_5)_2O\cdot BF_3$. Consequently, the strict requirements of (i) stoichiometric ratio of hardener/epoxide and (ii) a distribution of alternate epoxy- and hardener-loaded capsules might no longer be necessary for manufacturing self-healing epoxy composites. Only a few $(C_2H_5)_2O\cdot BF_3$ is sufficient for initiating crack healing.

Nevertheless, $(C_2H_5)_2O\cdot BF_3$ is highly hydroscopic and will lose its activity if conventional encapsulation approaches are applied. To solve the problem, the authors of the present work plan to try

* Corresponding author. Tel./fax: +86 20 84114008.
E-mail address: cesrmz@mail.sysu.edu.cn (M.Z. Rong).

0032-3861/$ – see front matter © 2008 Elsevier Ltd. All rights reserved.
doi:10.1016/j.polymer.2008.11.022

another method. First, polymeric hollow microcapsules are produced and then $(C_2H_5)_2O\cdot BF_3$ is infiltrated into the spheres. Activity of $(C_2H_5)_2O\cdot BF_3$ can thus be preserved.

Hollow microcapsules are gas-filled spherical particles with advantageous properties, like low effective density and high specific surface area. They are often used as opacifying plastic pigments for various coatings and gloss-enhancing plastic pigments, lightweight reinforcements, light scattering materials, etc. [26]. Fabrication of tailor-made hollow spherical structures has been carried out by many processes, including spray drying and dripping [27,28], emulsion/interfacial polymerization [29], self-assembling [30], etc. In general, template technique is involved. That is, microcapsules form with the core (liquid droplet or solid particle) as template. Subsequently, hollow spheres are acquired by decomposing the liquid or solid core either by dissolution, evaporation or thermolysis. It is worth noting that, however, capsules' shell used to be more or less damaged during the core decomposition [31–33].

In fact, when microbubble acts as the template, integrity of hollow microcapsules can be ensured. Of course, the formation rate of shell should be fast enough to encapsulate microbubbles before their disappearance, as the survival time of microbubbles in liquid is significantly shorter than that of dispersed liquid or solid cores. Harris et al. prepared hollow microcapsules from *n*-butyl-2-cyanoacrylate (NBCA) using microbubble template [34]. NBCA monomers can be rapidly polymerized on the surface of microbubbles in the presence of water. Daiguji et al. described a technique for generating hollow melamine-formaldehyde microcapsules via direct encapsulation of microbubbles [35]. Our laboratory developed a novel UV-irradiation method to produce microcapsules containing epoxy resin [36]. The distinct advantage of this method lies in its rapid reaction rate at room temperature, which just meets the requirement of the microbubble template technique stated above. Thereby, in this work hollow microcapsules are prepared by UV-initiated radical copolymerization in emulsion.

To facilitate the introduction of $(C_2H_5)_2O\cdot BF_3$ into the hollow microcapsules, performance of the polymeric wall should be optimized by proper choice of monomers. It is desired that the shell wall possesses similar polarity as $(C_2H_5)_2O\cdot BF_3$ for intimate contact between them. In addition, the microcapsules should be compatible with epoxy matrix and robust enough to withstand the manufacturing of epoxy composites in future applications. According to these criteria, the following monomers are chosen for building up the microcapsules: epoxydiacrylate, methyl methacrylate and monobutyl itaconate, while pentaerythritol triacrylates and 1,6-hexanediol diacrylates serve as the crosslink agents. The monomers are characterized by photosensitivity and compatibility with epoxy, and contain many polar groups (like hydroxyl, carbonyl and carboxylic groups).

Hereinafter, feasibility of the proposed approach, structure and properties of the resultant hollow microcapsules, and infiltration of $(C_2H_5)_2O\cdot BF_3$ into the capsules are discussed. Besides, reactivity of the encapsulated $(C_2H_5)_2O\cdot BF_3$ with epoxy is also verified.

2. Experimental

2.1. Materials

The monomers for shell making were epoxydiacrylate (E51-AA, homemade according to Ref. [36]), methyl methacrylate (MMA, supplied by Guangzhou Chemical Regents Co., China) and monobutyl itaconate (MBI, supplied by Guangzhou Shuangjian Trading Co., Ltd., China), respectively. The crosslinking agents, pentaerythritol triacrylates (PETA) and 1,6-hexanediol diacrylates (HDDA) were purchased from Tianjin Tian Jiao Chemical Industry Co. Ltd., China. The polymerizable emulsifier, sodium 3-methacryloyloxy-2-hydroxy propane sulphonate (HPMAS), was supplied by Guangzhou Shuangjian Trading Co., Ltd., China. Besides, the polymeric surfactant, poly(styrene–maleic sodium) (PSMS), was homemade referring to Ref. [36]. The blowing agent, methyl acrylic acid (MAA)/$NaHCO_3$, was provided by Guangzhou Chemical Co., China. The photo-initiator, 2-isobutoxy-2-phenyl-acetophenone (trade name: benzoin butyl ether), was purchased from Huntsman Co., China. $(C_2H_5)_2O\cdot BF_3$ was supplied by Changshu Yangyuan Chemical Engineering Co., China. Epoxy resin, diglycidyl ether of bisphenol A (trade name: E51), was purchased from Dongfeng Chemicals Co. Ltd., China. All the materials were used as-received without further purification. Fig. 1 shows chemical structures of the aforesaid photosensitive oligomers, crosslink agent, polymerizable emulsifier and photo-initiator.

2.2. Preparation of hollow microcapsules

The hollow microcapsules were prepared via UV-initiated radical copolymerization on microbubble template (Fig. 2). First, the monomers, crosslink agent, photo-initiator and blowing agent were mixed according to the recipes given in Table 1. Then, a gas–water emulsion was created by vigorously stirring surfactant aqueous solution (100 ml) containing dissolved $NaHCO_3$ (0.2 g), while dropping the above monomer mixtures within ~1 min. Afterwards, the resultant emulsion was homogenized at 1.2×10^4 rpm with a homogenizer for additional 5 min. Inside the Rayven UV oven (Intelli-Ray 400, USA), the emulsion was irradiated by UV light for 1–10 min under magnetic stirring at room temperature. The other synthetic parameters, like concentrations of surfactant and initiator, and UV lamp power, followed the optimum conditions worked out in our previous work [36].

By pouring the irradiated emulsion into 500 ml water, hollow microcapsules were floated and accumulated on the solution surface. They were collected by filtration, and washed with water and acetone alternately for several times to remove residual emulsifier, monomers and oligomers. At last, powder-like hollow microcapsules were obtained after drying in a vacuum freeze dryer. Yield of the hollow microcapsules was roughly estimated by the ratio of the resultant hollow microcapsules weight over the feeding weight of the wall formers.

To highlight the role of UV-initiated polymerization, a comparative experiment was carried out using a thermal initiator instead. The emulsion (100 ml) prepared according to recipe 3# (Table 1, excluding the photo-initiator) was charged into a three-necked flask (about 250 cc) fitted with a nitrogen bubbler, magnetic stir bar and condenser. Under protection of nitrogen and stirring at 500 rpm, 10 ml thermal initiator (0.6% ammonium persulfate water solution) was dropped to the emulsion. The reaction proceeded for 3 h at 70 °C. The product was poured into a large amount of water to remove the emulsifier. Then, the floating particles were collected by filtration, and washed with water and acetone alternately for several times, and finally dried in a vacuum freeze dryer.

2.3. Introduction of $(C_2H_5)_2O\cdot BF_3$ into hollow microcapsules

First of all, the gas (i.e. CO_2) inside the hollow microcapsules was evacuated for 1 h under vacuum circumstance. In addition, a $Ca(OH)_2$ solution was connected to the exporting pipeline to monitor whether CO_2 has been completely removed. After that, $(C_2H_5)_2O\cdot BF_3$ was vented into the system to submerge the microcapsules for 1–50 h. Eventually, the $(C_2H_5)_2O\cdot BF_3$-loaded microcapsules were obtained by filtration, and purged with ethyl-ether. The loading rate of $(C_2H_5)_2O\cdot BF_3$ in the hollow microcapsules was determined by chemical analysis as follows. The loaded microcapsules were ground and dispersed into water. Accordingly, the encapsulated $(C_2H_5)_2O\cdot BF_3$ was completely hydrolyzed:

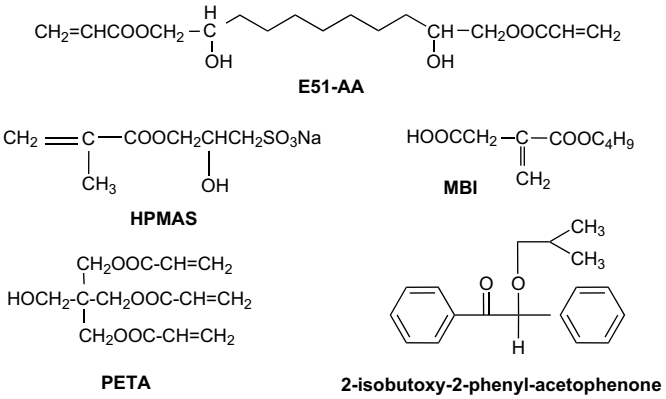

Fig. 1. Molecular structures of some chemicals used in this work.

$$(C_2H_5)_2O{\cdot}BF_3 = BF_3 + (C_2H_5)_2O \quad (1)$$

$$4BF_3 + 6H_2O = 3H_3O^+ + 3BF_4^- + B(OH)_3 \quad (2)$$

By measuring pH value of the solution with a pH meter (±0.05 pH), the weight of $(C_2H_5)_2O{\cdot}BF_3$ included in the hollow microcapsules was estimated from Eq. (3). As a result, the loading rate of $(C_2H_5)_2O{\cdot}BF_3$, α, was then obtained by Eq. (4).

Table 1
Recipes for preparing hollow microcapsules in emulsion via UV-irradiation method.[a]

Recipe ID	E51-AA (g)	MMA (g)	MBI (g)	HPMAS (g)	HDDA (g)
1#	3	0	0	3	0
2#	0	4	0	0	2
3#	0	2	0	3	1
4#	0	0	2	3	1

[a] PSMS: 3 wt%; PETA: 0.5 wt%; MAA: 2 wt%; photo-initiator: 0.5 wt% based on 100 ml water; agitation rate: 1.2×10^4 rpm (unless otherwise specified).

$$W = \frac{4}{3} \times \Delta\left[H^+\right] \times V \times M_{(C_2H_5)_2O{\cdot}BF_3} \quad (3)$$

$$\alpha = \frac{W}{W_0} \times 100\% \quad (4)$$

where W denotes the weight of $(C_2H_5)_2O{\cdot}BF_3$ loaded by the hollow microcapsules, $\Delta[H^+]$ is the difference in hydrogen ion concentration between the solutions containing ground $(C_2H_5)_2O{\cdot}BF_3$-loaded microcapsules and hollow microcapsules ($pH = -\lg[H^+]$), V is the volume of the consumed water (±0.1–0.2%), $M_{(C_2H_5)_2O{\cdot}BF_3}$ is the

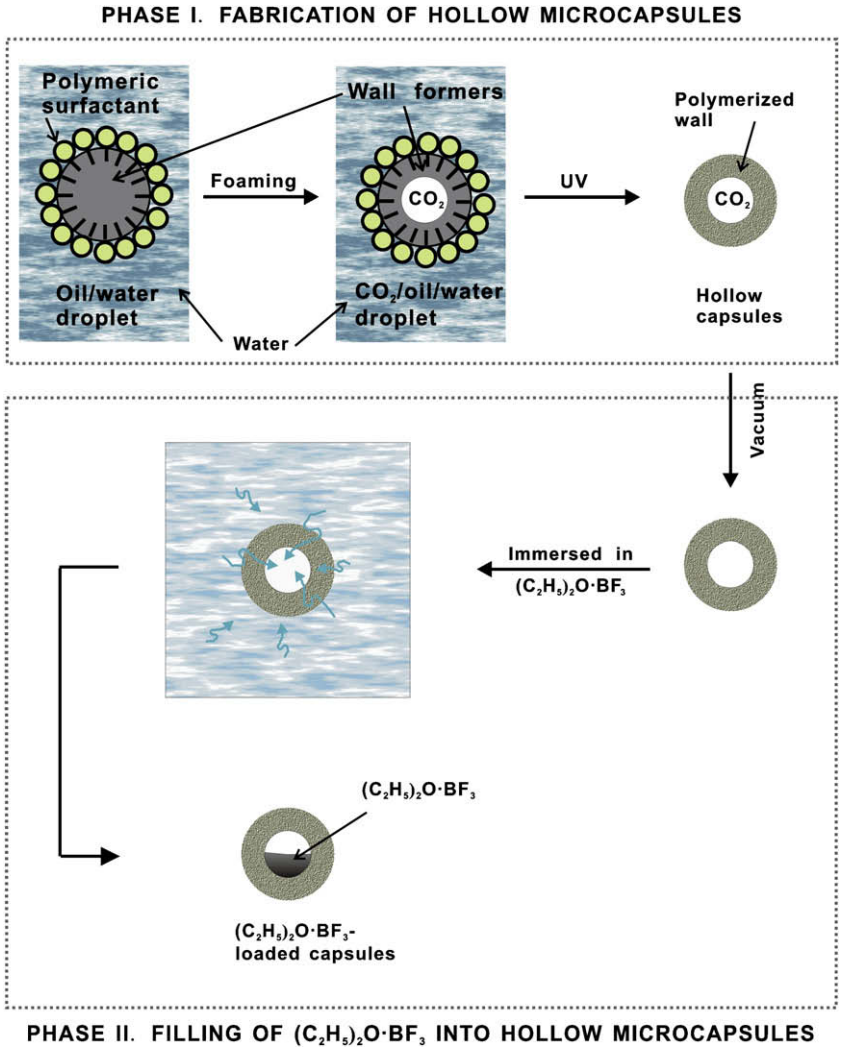

Fig. 2. Schematic drawing of the proposed route for preparing hollow microcapsules and filling $(C_2H_5)_2O{\cdot}BF_3$ into hollow microcapsules.

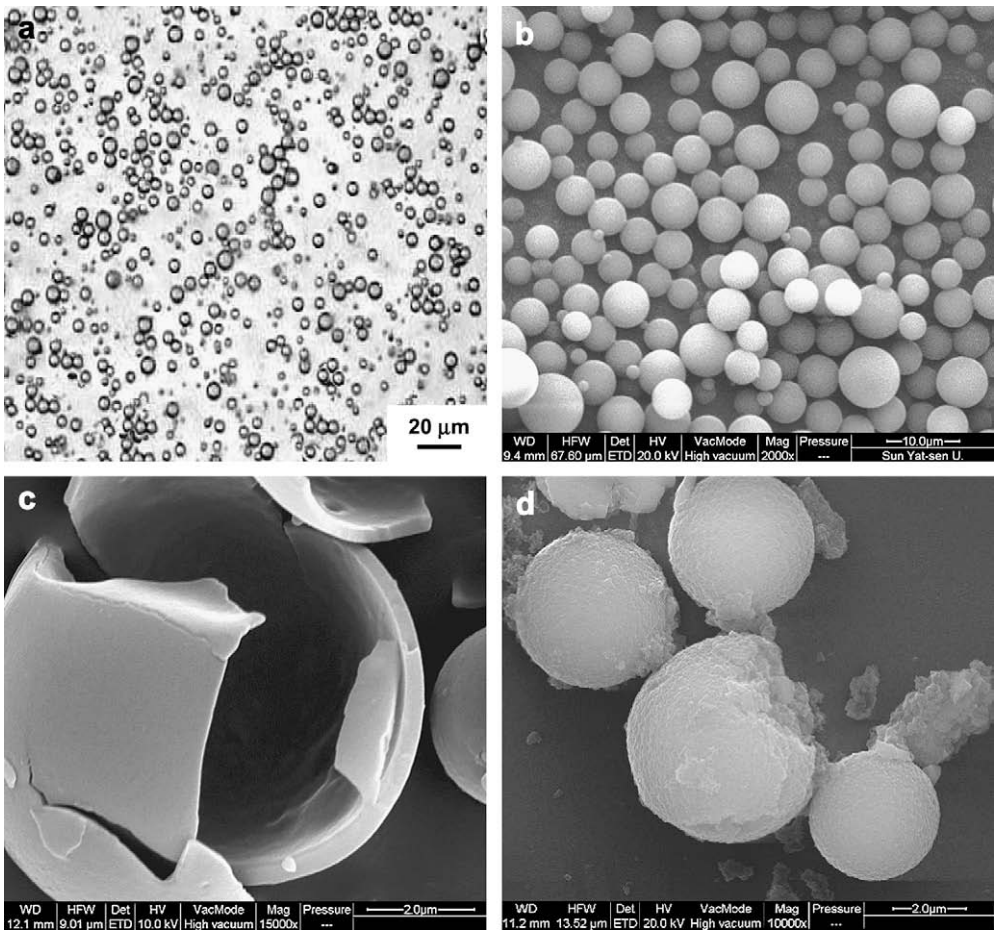

Fig. 3. (a) Optical micrograph of microbubbles in CO_2/oil/water emulsion; (b) SEM micrograph of hollow microcapsules made by UV-initiated polymerization; (c) SEM micrograph of crushed microcapsules made by UV-initiated polymerization; (d) SEM micrograph of solid microspheres made by thermally initiated polymerization. Recipe: (a)–(c) 3#; (d) 3# except that the photo-initiator was replaced by a thermal initiator (see Section 2).

molecular weight of $(C_2H_5)_2O{\cdot}BF_3$, and W_0 is the weight of the hollow microcapsules before loading $(C_2H_5)_2O{\cdot}BF_3$.

2.4. Characterization

An optical method was used to evaluate the evolution of microbubbles in liquid. The microbubble suspension was diluted with water and dropped onto a glass plate, which was then covered by a cover glass and observed with an optical microscope and a CCD camera (MS, PM-T3, Olympus). Surface morphology and cross section of the hollow microcapsules were viewed by a scanning electronic microscope (SEM, Philips XL30-FEG), while their size distribution was measured using a MasterSize 2000 laser scattering size analyzer. Composition of the hollow microcapsules'

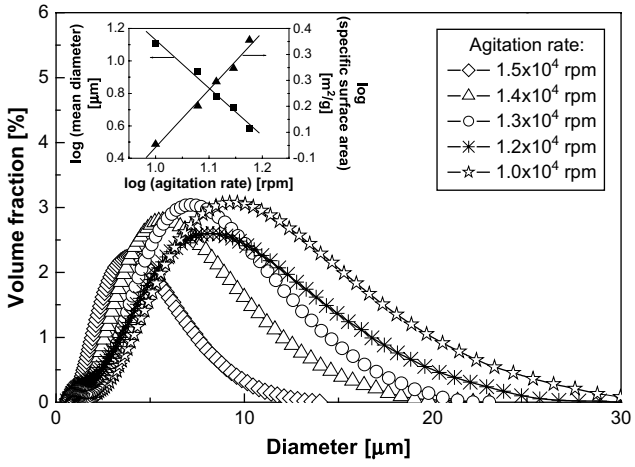

Fig. 4. Influence of agitation rate on size distribution of hollow microcapsules (recipe: 3#). The inset shows log–log dependences of mean diameter and specific surface area of hollow microcapsules on agitation rate.

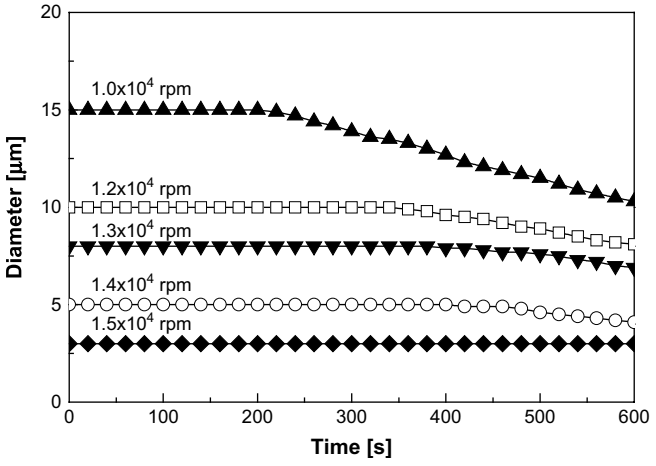

Fig. 5. Size evolution of single microbubbles (recipe: 3#) generated at different stirring rates as a function of time.

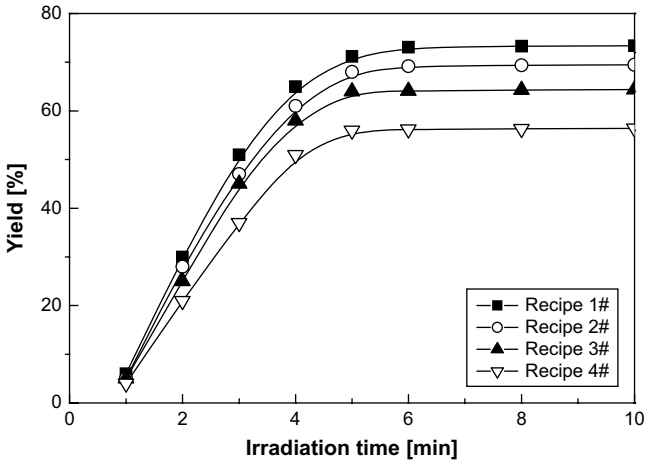

Fig. 6. Yields of hollow microcapsules as a function of UV-irradiation time.

shell and reactivity of the loaded $(C_2H_5)_2O{\cdot}BF_3$ were characterized by a Nexus 670 Fourier transform infrared (FTIR) spectroscope. Surface free energy of the hollow microcapsules was measured by a Kruss K12 Tensiometer at room temperature according to Owens–Wendt–Rabel–Kaelble method [37]. Micropore and mesopore size distributions of the shell walls were determined by an ASAP 2010 Micromeritics accelerated surface area and porosimetry system.

3. Result and discussion

3.1. Formation of hollow microcapsule

As shown in Fig. 2, the key step prior to UV-irradiation is the formation of microbubbles, which are surrounded with a monomer layer and stabilized by surfactant. To achieve this objective, a special blowing system consisting of MAA and $NaHCO_3$ was applied. It is able to give out CO_2 as a result of the reaction between the two components. In practice, MAA was mixed with monomers in advance, while $NaHCO_3$ was dissolved in water. As the mixture of the monomers was dropped into the surfactant water under stirring, an emulsion of monomers (oil/water) formed accordingly. In the meantime, MAA in the monomer mixture tend to be dissolved in water due to its water solubility, and minute amounts of water diffused into the oil phase. As soon as MAA contacted $NaHCO_3$, a large amount of microbubbles was generated just inside the droplets of the monomer mixture or at the oil/water interface. Consequently, the original monomer emulsion (oil/water) turned to a CO_2/oil/water one. Although a few oil droplets might remain unchanged during the foaming process, they were likely absorbed by the oil layer of the CO_2/oil/water droplets, because the latter possessed large specific surface area and were miscible with the monomers. Fig. 3(a) shows an example of such emulsion. Evidently, most droplets are CO_2/oil/water ones.

Having been irradiated by UV light, polymerization of the monomers took place and hollow microcapsules were produced. Fig. 3(b) indicates that the capsules have relatively uniform size (2–10 μm), which is similar to that of the microbubble templates (Fig. 3(a)). This suggests that the shell was successfully in situ consolidated before the microbubbles lost their stability. On the other hand, destruction of the capsules by mechanical agitation was not found for these collected floating microcapsules, meaning that the wall was rather strong. Fig. 3(c) illustrates the artificially crushed microcapsules. Hollow structure (filled with CO_2) rather than solid particle or porous structure can be identified. The wall thickness is estimated as 200–300 nm for a sphere 8 μm in diameter.

Influence of shear on size of the hollow microcapsules was studied. As the stirring speed increased from 1.0×10^4 to 1.5×10^4 rpm during the formation of CO_2/oil/water emulsion, the capsules became obviously smaller and the size distribution also narrowed (Fig. 4). The inset of Fig. 4 further shows the linear reduction in mean diameter with stirring speed on log–log axes, while the specific surface area varies inversely. The results manifest that the hollow microcapsules can retain the original microbubbles' size so long as the microbubbles keep stable during the hardening process.

To clarify the relationship between the microbubbles' and hollow microcapsules' sizes, the microbubbles generated at different stirring speeds were monitored. Clearly, the microbubbles' size is decreased with a rise in stirring speed (Fig. 5), which coincides with the results of Fig. 4. Moreover, since CO_2 would gradually diffuse into water, all the microbubbles have a tendency to decrease their sizes with time. Comparatively, the smaller microbubbles in the aqueous solution are more stable than the larger ones. On the whole, so long as the shell formation via UV-initiated polymerization is completed within 5 min, solidified hollow structure of the microbubbles can be obtained. Otherwise, the resultant hollow microcapsules might be much smaller than the initial microbubbles.

Fig. 6 gives the dependencies of yield of the hollow microcapsules on UV-irradiation time. For all the systems, the yields increase quickly within the first several minutes and then level off. Actually, each system attains its highest yield at about 5 min, which just falls in the stable stage of microbubbles (see Fig. 5). The absence of induction period at the early stage of polymerization resulting from the specific photo-initiator [36] must have made the critical contribution to this favorite result.

On the other hand, the equilibrium yields of the hollow microcapsules range between 56 and 73% (Fig. 6), indicating that a certain amount of monomer droplets have not been turned into microbubbles covered with the oil layer during blowing. In addition, these monomer droplets might prefer to stay in the bulk solution rather than to immigrate into the oil layer of microbubbles. After UV-irradiation, they were converted into solid spheres and sank in the solution. There is another possibility that some monomers were dissolved in water, and polymerized in the solution. Also, the broken capsules would be precipitated in the solution.

Table 2
Three-dimensional solubility parameters of MMA and E51-AA in comparison with those of water[a] (unit: $J^{1/2}/cm^{3/2}$).

Substance	δ_d[b]	δ_p[c]	δ_h[d]	$\lvert\delta_{d,monomer} - \delta_{d,H_2O}\rvert$	$\lvert\delta_{p,monomer} - \delta_{p,H_2O}\rvert$	$\lvert\delta_{h,monomer} - \delta_{h,H_2O}\rvert$
MMA	18.0	5.2	8.6	5.0	26.1	25.6
E51-AA	19.8	2.9	12.3	6.8	28.4	21.9
H_2O	13.0	31.3	34.2	–	–	–

[a] The solubility parameters of water are cited from Ref. [38], while those of the monomers are estimated by the group contribution method [38].
[b] δ_d: Dispersive or non-polar component of solubility parameter.
[c] δ_p: Polar component of solubility parameter.
[d] δ_h: Hydrogen bonding component of solubility parameter.

Fig. 6 also shows that the equilibrium yields of the hollow microcapsules are different for different recipes. As the system without polymerizable emulsifier HPMAS (recipe 2# in Table 1) still presents a higher yield, dosage of the emulsifier might not be the key factor. Naturally, monomers' solubility in water is considered. It is seen from Fig. 6 that recipe 3# containing MBI offers the lowest equilibrium yield. MBI is a water-soluble monomer owing to its carboxyl acid group, and can act as a blowing agent by reacting with $NaHCO_3$. Its reactant MBINa (product of the reaction between MBI and $NaHCO_3$) is also soluble in water. These are certainly detrimental to the production of hollow microcapsules. In contrast, epoxydiacrylate and methyl methacrylate are basically water-insoluble substances. The difference in the polar component of solubility parameter between the monomer and water, $|\delta_{p,monomer} - \delta_{p,H_2O}|$, is more remarkable in the case of epoxydiacrylate (Table 2). As water is a strong polar solvent, similarity in δ_p between water and its solute is closely related to the dissolution. It suggests that diffusion of epoxydiacrylate monomers into water might be more difficult as compared with methyl methacrylate, so that recipe 1# exhibits the highest equilibrium yield (Fig. 6). In fact, the difference in the equilibrium yields between recipes 2# and 3# provides supporting evidence for the above analysis. Since methyl methacrylate has poor water solubility, an increase in its concentration in the system would increase the hydrophobicity. Hence the equilibrium yield of recipe 2# is higher than 3#.

To understand the effect of blowing agent, a control experiment was conducted, in which recipe 3# in Table 1 without MAA/$NaHCO_3$ was used. The equilibrium yield of the hollow microcapsules was only 7%, indicating that the in-situ generated CO_2 by blowing agent plays a key role in producing hollow microcapsules through forming CO_2/oil/water emulsion. On the contrary, the contribution of monomer coated, entrained air bubbles is limited. Another important factor in the synthesis of hollow microcapsules lies in the surfactant dissolved in water. Stabilization of microbubbles is more difficult than that of monomers droplets. Thereby, a macromolecular surfactant, PMSM, was employed to form a stronger film surrounding the microbubbles, and stabilize the microbubbles for a longer time. Low-molecular weight surfactants, such as Tween-40, Span-40, sodium dodecyl sulfonate and sodium dodecyl benzene sulfonate, were also tried, but failed to produce hollow microcapsules.

The hollow microcapsules' size and wall thickness are affected by the feeding concentration of wall formers. In the case of a given group of components (refer to recipe 3# in Table 1), the influence of feeding concentration of wall formers on average radius, r, wall thickness, w, and aspect ratio $A(=r/w)$ of resultant hollow microcapsules is exhibited in Fig. 7. It is seen that the aspect ratio decreases with increasing feeding concentration of wall formers despite the fact that both average radius and wall thickness change in an opposite way. In general, a thicker wall can be attributed to the fact that a larger amount of monomer was absorbed on the oil layer of microbubbles. Meanwhile, a thicker oil layer would help to stabilize CO_2/oil/water droplets, leading to a larger capsule. The gradually descending aspect ratio manifests that the increase in capsules' wall thickness is faster than that in their size. Nevertheless, the aspect ratios are not high (6.4–7.5), meaning that the hollow microcapsules possess quite large cavity with relatively thin wall.

On the whole, the approach based on UV-irradiation polymerization proves to be effective in producing hollow microcapsules. When the photo-initiator was replaced by a thermal initiator (i.e. $(NH_4)S_2O_8$), much longer time ($\sim$2 h) was needed for the appearance of microspheres and most of them are solid (Fig. 3(d)). This is because during long time thermal polymerization the microbubbles tended to either disappear or only hold a small amount of

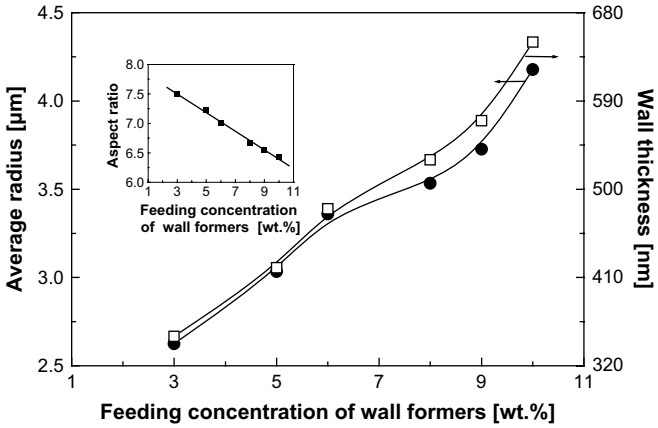

Fig. 7. Dependences of average radius, wall thickness, and aspect ratio of hollow microcapsules on feeding concentration of wall formers. Here the hollow microcapsules were synthesized using the components described in recipe 3# (Table 1) and the feeding weight ratio among the components was also fixed, following that of recipe 3#.

CO_2. Thus, the yield of hollow microcapsules after reaction for 3 h was as low as 20%, and the mean diameter is significantly larger than that of the capsules made by UV-irradiation (Fig. 8).

3.2. Filling of $(C_2H_5)_2O{\cdot}BF_3$ into hollow microcapsules

As mentioned in Section 1, the hollow microcapsules are made to hold $(C_2H_5)_2O{\cdot}BF_3$ for application as a sealed self-healing agent. It is thus necessary to tailor the wall features for optimum loading. Fig. 9 gives FTIR spectra of the capsules' walls. Distinguished absorption peaks of sulfonic group at 1250 and 1050 cm^{-1} are observed for the microcapsules prepared according to recipes 1#, 3# and 4#, demonstrating that HPMAS has been incorporated in the shell. Multi-peaks in relation to phenyl ring of bisphenol A at 1600, 1585, 1500 and 1450 cm^{-1} in association with the peak of carbonyl group at 1745 cm^{-1} confirm that the capsules from recipe 1# are made by epoxydiacrylate. For the capsules based on recipes 2#, 3# and 4#, in which HDDA molecules are included, the characteristic peak at 720 cm^{-1} corresponding to the group of $-(CH_2)_n-$ ($n \geq 4$) is perceivable. In addition, the evident carbonyl peaks at 1745 and 1760 cm^{-1} also appear on the spectra of these samples.

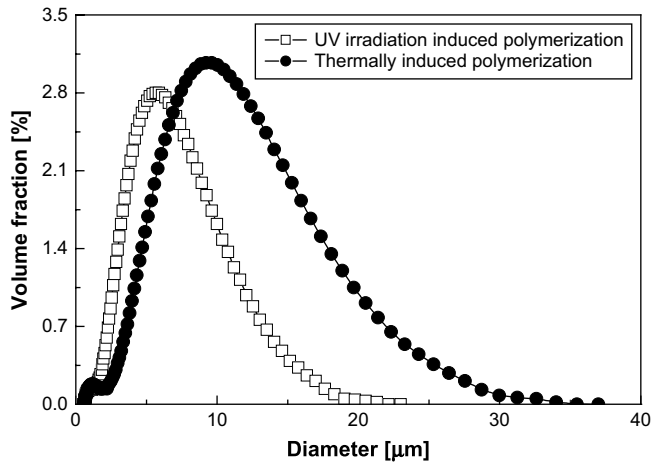

Fig. 8. Size distribution of microcapsules prepared by UV-initiated polymerization (recipe: 3#) and thermally initiated polymerization (recipe: 3#, except that the photo-initiator was replaced by a thermal initiator, see Section 2). Agitation rate: 1.4×10^4 rpm.

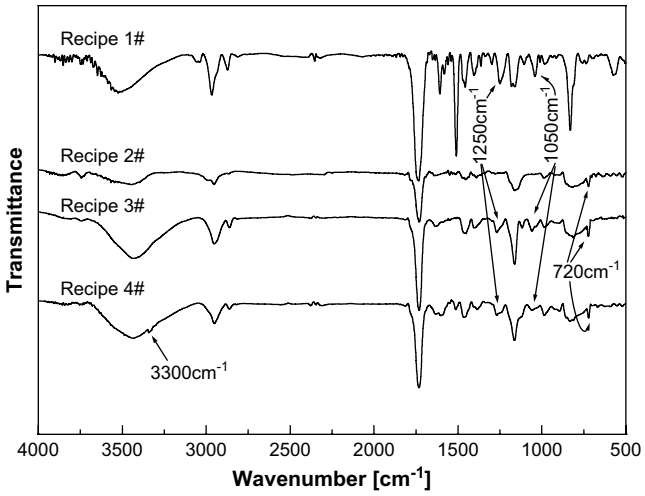

Fig. 9. FTIR spectra of hollow microcapsules.

Especially, a small carboxyl peak at 3300 cm^{-1} is distinguished for the microcapsules from recipe 4#, implying that MBI has been attached to the shell. Characteristic absorption peaks of hydroxyl group at 3500 cm^{-1}, and methyl and methylene at 2960 and 2870 cm^{-1} are visible for the four types of hollow microcapsules. From the above analysis, it is concluded that the hollow microcapsules designed by the recipes in Table 1 have been produced as expected.

Besides chemical structures, geometry and morphology of the hollow microcapsules also affect infiltration of $(C_2H_5)_2O{\cdot}BF_3$. Although it has been known that the capsules have thin wall (Fig. 3(c)), which is beneficial to the loading of $(C_2H_5)_2O{\cdot}BF_3$, a careful inspection of the capsules' appearance should be conducted. As shown in Fig. 10, surface of the microcapsule resulting from recipe 2# (Fig. 10(b)) is smoother and more compact than those of the microcapsules containing HPMAS (Fig. 10(a), (c) and (d)). The former is only composed of hydrophobic monomers MMA and HDDA, and apt to contract after polymerization. On the other hand, HPMAS must have been assembled at the surface of microbubbles with their hydrophilic groups (like $-SO_3Na$ and hydroxyl) toward the aqueous phase. As a result, surface of the hollow microcapsule with HPMAS became coarse due to the extension of the HPMAS molecules when the capsules were built up. With respect to the microcapsule derived from recipe 4# (Fig. 10(d)), MBI also took the effect of polymerizable emulsifier and hence the capsule's surface roughness has been further increased.

Since the hollow microcapsules are made from the materials that are compatible with $(C_2H_5)_2O{\cdot}BF_3$, the ones with rougher surface representing loose accumulation of molecules should favor infiltration of $(C_2H_5)_2O{\cdot}BF_3$, as intuitively expected. The loading curves of the hollow capsules shown in Fig. 11 demonstrate it is the case. With a rise in infiltration time, the loading rate is gradually increased until the equilibrium at 14–24% is reached after 40 h. The capsules made from recipe 4# are indeed filled with much more $(C_2H_5)_2O{\cdot}BF_3$ than the others. The smooth capsules from recipe 2# have the lowest equilibrium loading rate. The data show that the proposed route for making hollow microcapsule works, and the

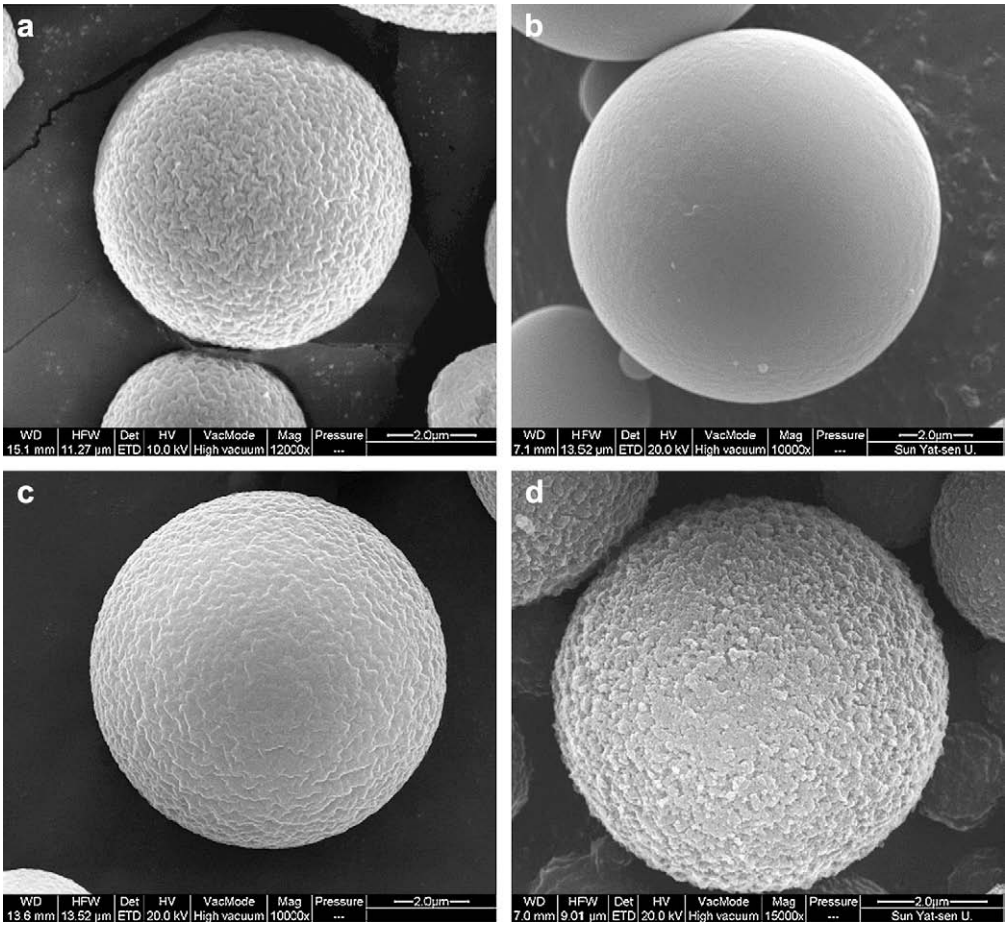

Fig. 10. SEM micrographs of hollow microcapsules derived from (a) recipe 1#, (b) recipe 2#, (c) recipe 3#, and (d) recipe 4#.

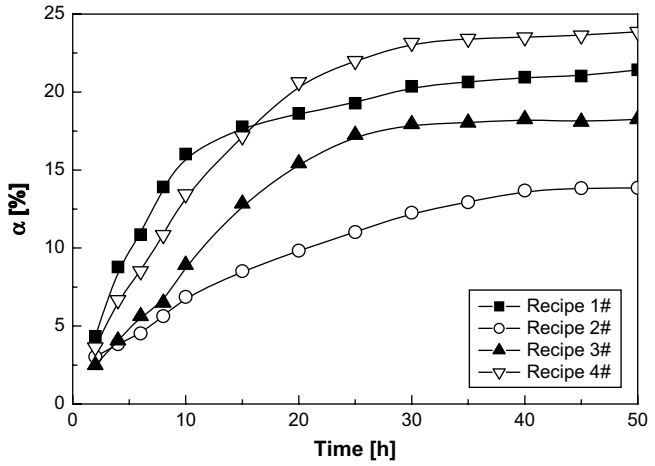

Fig. 11. Loading rate of $(C_2H_5)_2O{\cdot}BF_3$ in hollow microcapsules as a function of immersion time.

loading amount of $(C_2H_5)_2O{\cdot}BF_3$ in the capsules can be adjusted by changing the shell composition.

To find out the reason for the different equilibrium loading rates of different microcapsules, the porous characteristics of the walls of the hollow microcapsules was examined by nitrogen adsorption isotherms at liquid nitrogen temperature. Both mesopores and micropores are recognized on the wall surface (Fig. 12), which should have important contribution to the infiltration of $(C_2H_5)_2O{\cdot}BF_3$. Actually, the detected pores of all the capsules' walls range from several to hundreds angstrom. They are large enough for the travel of $(C_2H_5)_2O{\cdot}BF_3$, because the latter' size is about 6.86 Å. It seems that the pores' content plays a critical role. Fig. 12 exhibits that the amounts of mesopores and micropores in the range of interests decrease in the sequence of recipes 1#, 4#, 3# and 2#. By surveying Fig. 11, it is evident that the hollow microcapsules from recipes 1# and 4# with more pores facilitate infiltration of $(C_2H_5)_2O{\cdot}BF_3$, while those from recipes 3# and 2# having fewer pores are bound to exert negative effect on the loading. However, a careful observation of Fig. 11 and Fig. 12 further reveals that the microcapsules from recipe 4# have higher equilibrium loading rate than those from recipe 1#, despite the fact the former possesses less pores than the latter. There might exist some other things which influence the loading performance. Accordingly, surface chemistry should be analyzed.

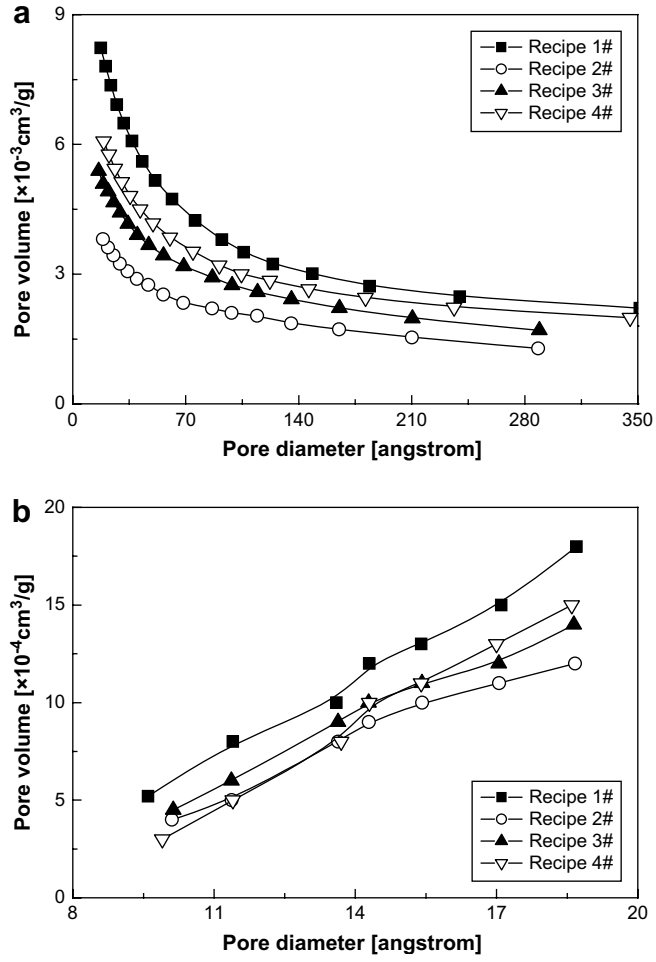

Fig. 12. Size distribution of the pores on the surface of hollow microcapsules: (a) mesoporous, and (b) microporous.

Table 3
Surface free energies of the hollow microcapsules.

Recipe ID	Surface free energy[a] (mJ/m^2)	
	γ^d	γ^p
1#	34.1	9.0
2#	27.3	5.2
3#	31.9	7.7
4#	33.9	10.9

[a] γ^d: dispersive component of surface free energy; γ^p: polar component of surface free energy.

It is known that boron trifluoride diethyl etherate is a polar molecule. Therefore, various polar groups, such as –COOH, –SO_3Na, –OH and –COOR, were introduced onto the shell of the capsules, respectively (Fig. 1). Although the wall formers have met the requirement for molecular miscibility between the capsules and $(C_2H_5)_2O{\cdot}BF_3$, surface characteristics of the capsules has not yet been quantified. For this purpose, Table 3 lists surface free energies of the hollow microcapsules. It is interesting to see that dispersive component of surface free energy, γ^d, and polar component of surface free energy, γ^p, of the microcapsules rank in different orders: recipes 1# > 4# > 3# > 2# for γ^d and recipes 4# > 1# > 3# > 2# for γ^p. The former sequence resembles that of the pore content (Fig. 12), while the latter sequence is similar to that of the loading ability of the hollow microcapsules (Fig. 11). It implies that

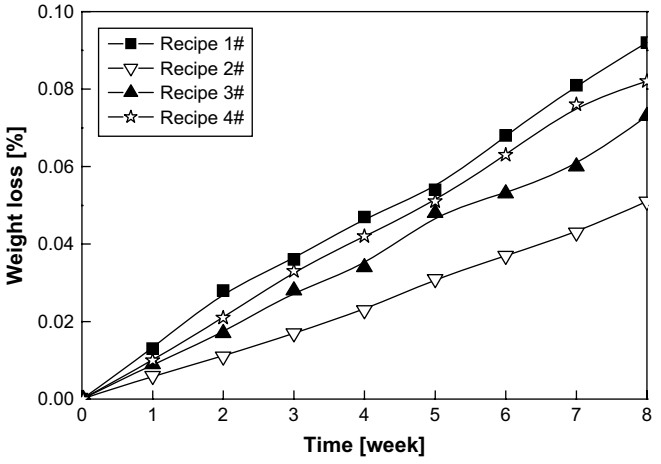

Fig. 13. Weight loss of $(C_2H_5)_2O{\cdot}BF_3$-loaded microcapsules as a function of time at room temperature. Initial loading rates of $(C_2H_5)_2O{\cdot}BF_3$: recipe 1#, 20 wt%; recipe 2#, 13 wt%; recipe 3#, 18%; recipe 4#, 22 wt%.

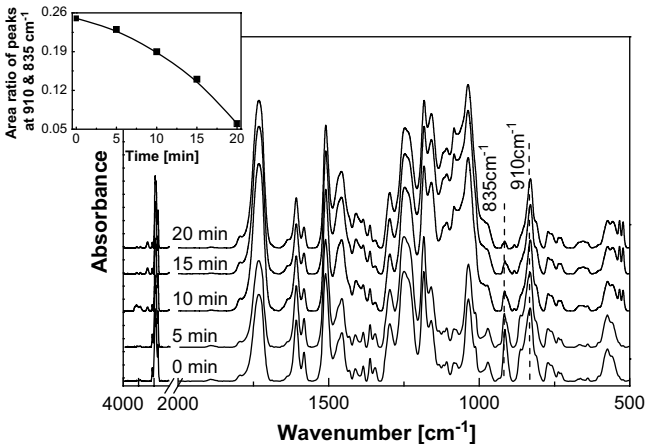

Fig. 14. In-situ FTIR spectra tracking the reaction between epoxy and ground $(C_2H_5)_2O\cdot BF_3$-loaded microcapsules (recipe 3# in Table 1; loading rate: 18%). The inset shows the peak area ratio of epoxide group to phenyl ring as a function of time.

higher polarity of the capsules' wall leads to higher equilibrium loading of $(C_2H_5)_2O\cdot BF_3$. The phenomenon should be related with the interaction between the polar groups and $(C_2H_5)_2O\cdot BF_3$. Detailed mechanism will be investigated in the future.

On the other hand, there might exist a reverse infiltration of $(C_2H_5)_2O\cdot BF_3$ from the $(C_2H_5)_2O\cdot BF_3$-loaded microcapsules, which determines service life of the microcapsules. Accordingly, weight loss of the microcapsules stored at room temperature was recorded as a function of time (Fig. 13). It is evident that the weight loss is very few (e.g., less than 0.1 wt% for 2 months). That is, the reverse infiltration proceeds very slowly and $(C_2H_5)_2O\cdot BF_3$ in the microcapsules can be used for long time. Such a low reverse infiltration rate relative to the infiltration rate can be understood from the different environments during filling of hollow microcapsules and storage of $(C_2H_5)_2O\cdot BF_3$-loaded microcapsules. As mentioned in Section 2, the gas (i.e. CO_2) inside the hollow microcapsules was evacuated under vacuum before infiltration of $(C_2H_5)_2O\cdot BF_3$, which led to a high infiltration rate within short time. However, the reverse infiltration has to be carried out under atmosphere pressure, so that very slow weight loss was perceived.

3.3. *Reactivity of microencapsulated $(C_2H_5)_2O\cdot BF_3$*

Since $(C_2H_5)_2O\cdot BF_3$ is a highly active agent, it should be known whether the filled version in the microcapsules keeps its chemical activity. Accordingly, in-situ FTIR spectroscopy was used to study the reaction of epoxy resin (E51) coated on the surface of KBr tablet containing ground $(C_2H_5)_2O\cdot BF_3$-loaded hollow microcapsules (Fig. 14). It is seen that the characteristic peak of epoxide groups at 910 cm^{-1} diminishes with time. When the peak area of phenyl ring at 835 cm^{-1} serves as the internal standard, the peak area ratios of epoxide group to phenyl ring can be used to estimate the reaction degree (see the inset of Fig. 14). Evidently, about 80% epoxide groups are consumed within 20 min at room temperature. The results suggest that the encapsulated $(C_2H_5)_2O\cdot BF_3$ should be able to act as the hardener of uncured epoxy for crack healing in epoxy composites. More details of its healing ability will be reported in a future paper of the authors.

4. Conclusions

Hollow microcapsules for storing $(C_2H_5)_2O\cdot BF_3$ were successfully prepared by means of UV-initiated radical copolymerization in microbubble emulsion. The key steps lay in that (i) formation of CO_2/oil/water droplets, and (ii) rapid polymerization of the wall formers under UV-irradiation. Addition of blowing agent provided the system with much more CO_2 microbubbles than conventional mechanical stirring. Only macromolecular surfactant rather than low-molecular weight surfactants were qualified for stabilizing the CO_2/oil/water droplets. The selected photo-initiator guaranteed completion of the capsules' wall solidification before the bubbles lost their stability. The resultant microcapsules' shell wall was relatively thin (~0.2 μm), which assured sufficient space for holding $(C_2H_5)_2O\cdot BF_3$ even the microcapsules were very small (1–10 μm). It was revealed that the capsules' size and size distribution were mainly determined by dispersion rate, while the yield depended on solubility of the monomers in water. The aspect ratio gradually descended with a rise in feeding concentration of wall formers.

Structure and properties of the hollow microcapsules can be tailored by using different monomers. The hydrophilic monomers resulted in coarser surface morphology and more pores on the shell, which were beneficial to the infiltration of $(C_2H_5)_2O\cdot BF_3$. In addition, the shell wall with higher polarity increased the loading rate of $(C_2H_5)_2O\cdot BF_3$ in the microcapsules. The encapsulated $(C_2H_5)_2O\cdot BF_3$ kept its reactivity with epoxy as expected.

Acknowledgements

The authors are grateful to the support of the Natural Science Foundation of China (Grants: 50573093, U0634001 and 20874117).

References

[1] Wool RP. Soft Matter 2008;4:400.
[2] Yuan YC, Yin T, Rong MZ, Zhang MQ. Express Polym Lett 2008;2:238.
[3] White SR, Sottos NR, Geubelle PH, Moore JS, Kessler MR, Sriram SR, et al. Nature 2001;409:794.
[4] Brown EN, Sottos NR, White SR. Exp Mech 2002;42:4372.
[5] Brown EN, White SR, Sottos NR. J Mater Sci 2004;39:1703.
[6] Rule JD, Sottos NR, White SR, Moore JS. Educ Chem 2005;42(5):130.
[7] Rule J, Brown EN, Sottos NR, White SR, Moore JS. Adv Mater 2005;72:205.
[8] Jones AS, Rule JD, Moore JS, White SR, Sottos NR. Chem Mater 2006;18:1312.
[9] Kessler MR, White SR. Compos Part A Appl Sci 2001;32:5683.
[10] Kessler MK, Sottos NR, White SR. Compos Part A Appl Sci 2003;34:743.
[11] Brown EN, White SR, Sottos NR. Compos Sci Technol 2005;65:2466.
[12] Brown EN, White SR, Sottos NR. Compos Sci Technol 2005;65:2474.
[13] Jones AS, Rule JD, Moore JS, Sottos NR, White SR. J R Soc Interface 2007;4:395.
[14] Wilson GO, Moore JS, White SR, Sottos NR, Andersson HM. Adv Funct Mater 2008;18:44.
[15] Rule JD, Sottos NR, White SR. Polymer 2007;48:3520.
[16] Keller MW, White SR, Sottos NR. Polymer 2008;49:3136.
[17] Yin T, Rong MZ, Zhang MQ, Yang GC. Compos Sci Technol 2007;67:201.
[18] Rong MZ, Zhang MQ, Zhang W. Adv Compos Lett 2007;16:167.
[19] Yin T, Zhou L, Rong MZ, Zhang MQ. Smart Mater Struct 2008;17:015019.
[20] Yuan L, Liang GZ, Xie JQ, Li L, Guo J. Polymer 2006;47:5338.
[21] Satosdhi M, Ikuzo U, Makoto K, Kunihiko N. E.U. Patent 0,543,675; 1993.
[22] Ronald LH, Dale EW, Colin ED. U.S. Patent 4,536,524; 1985.
[23] Yuan YC, Rong MZ, Zhang MQ. Acta Polym Sin 2008;(4):472 [in Chinese].
[24] Yuan YC, Rong MZ, Zhang MQ. Polymer 2008;49:2531.
[25] Yuan YC, Rong MZ, Zhang MQ, Chen J, Yang GC, Li XM. Macromolecules 2008;41:5197.
[26] Ma GH, Chen AY, Su ZG, Omi S. J Appl Polym Sci 2003;87:244.
[27] Netting DI. U.S. Patent 3,794,503; 1974.
[28] Sands BW. U.S. Patent 4,421,562; 1983.
[29] Omi S, Katami K, Yamamoto A, Iso M. J Appl Polym Sci 1994;51:1.
[30] Fujimoto K, Toyoda T, Fukui Y. Macromolecules 2007;40:5122.
[31] Velev OD, Furusawa K, Nagayama K. Langmuir 1996;12:2374.
[32] Yang M, Ma J, Niu ZW, Dong X, Xu H, Meng Z, et al. Adv Funct Mater 2005;15:1523.
[33] Hu YX, Ge JP, Sun Y, Zhang TR, Yin YD. Nano Lett 2007;7:1832.
[34] Harris JR, Depoix F, Urich K. Micron 1995;26:103.
[35] Daiguji H, Makuta T, Kinoshita H, Oyabu T, Takemura F. J Phys Chem B 2007;111:8879.
[36] Xiao DS, Rong MZ, Zhang MQ. Polymer 2007;48:4765.
[37] Owens DK, Wendt RC. J Appl Polym Sci 1969;13:1741.
[38] van Krevelen DW. Properties of polymers. 3rd ed. Amsterdam: Elsevier; 1990.